APPLICATION OF THE VARIABLE-FIDELITY MDO TOOLS TO A JET AIRCRAFT DESIGN

Keita Hatanaka*, Shigeru Obayashi, Shinkyu Jeong****
** Mitsubishi Heavy Industries, Ltd., 10, Oye-Cho, Minato-Ku, Nagoya, 455-8515, Japan*
*** Tohoku University Katahira 2-1-1, Aoba-Ku, Sendai, 980-8577, Japan*

Keywords: *MDO, Variable-Fidelity, NURBS, engine-airframe integration*

Abstract

A 5-year R&D project has been in progress in Japan toward the development of an environmentally friendly high performance small jet aircraft since 2003. We developed and applied a Multidisciplinary Design Optimization (MDO) tool to a wing design in the conceptual design phase where a block fuel optimization was performed through aero and structural optimization. To be used as a practical design tool, we have introduced a flexible airfoil representation method to ensure a sufficient design space, and an optimization acceleration method to obtain the optimum in the practical time. As a result, by applying the CAD based geometry representation method and the Variable-Fidelity method to our MDO tool, the expansion of the design space was achieved and the optimization time was reduced to 10%. These techniques were applied to an engine-airframe integration, which is one of the most important items of the airplane design.

1 Introduction

In Japan, a 5 year R&D project has been in progress toward the development of an environmentally friendly high performance small jet aircraft aiming for a generation of the new industries under auspice from NEDO [1] (New Energy Development Organization) since 2003, in which new technical features have been investigated including advanced aerodynamics, new materials and so on. Mitsubishi Heavy Industries, Ltd. (MHI) is in charge of the aerodynamic design as a prime contractor of the project.

In this program, we developed a multi disciplinary optimization (MDO) tool by coupling a high-fidelity aerodynamic evaluation method such as Navier-Stokes solver with a genetic algorithm (GA) through a joint R&D study between MHI and Tohoku University [2]. However, there still remained some concerns about the design space definition and the computational cost in chapter 2.

To overcome these concerns and to perform wing-body design optimization, we introduced two new techniques in our MDO tool. The first was a flexible geometry representation method based on the Non-Uniform Rational B-Spline (NURBS)[3] technique, which was used in the CAD field, and the second was the effective optimization tool based on the Variable-Fidelity technique. By applying these techniques to our optimization tool, both the expansion of the design space and the acceleration of the optimization were achieved in the preliminary design phase.

Then we extended this MDO tool to a much complicated and practical engine-airframe integration problem as a next step. To overcome not only an aerodynamic complexity but also the trade-off among other features such as weight, flutter etc, an automatic and robust mesh generator for wing-body-nacelle geometries were developed.

2 Wing-Body design optimization

2.1 Airfoil representation method

In the MDO, the adequacy of the design space of an optimization problem strongly affects whether we can reach practically enough

optimized solution or not. Especially in the wing optimization problem, the most dominant factor is how to define the wing shape. In the optimization field, many airfoil shape representation methods have been developed such as discrete point representation method, polynomial function, partial polynomial function expression and CAD based expression method [4]. However, some methods cannot represent transonic airfoils precisely because of the large camber and curvature around the leading edge. Though the way of the definition of the airfoil shape is most important, there is still no general way.

In our previous work, we applied the PARSEC [5] method for the airfoil shape representation. However, we could not reach the optimized solution whose high speed drag was smaller than that of the airfoil designed by the conventional way based on the experience and knowledge of the engineer. It was assumed that the PARSEC method did not contain the true optimized solution in its design space.

Nowadays, a NURBS (Non-Uniform Rational B-Spline) is widely used in the CAD area and it has the capability of modifying the geometry locally. After investigation on the improvement of the airfoil shape definition we apply the NURBS method to enhance the flexibility of an airfoil shape. NURBS expression is shown below.

$$T = [t_0 \quad t_1 \quad \cdots \quad t_{m+n-1}] \tag{1}$$

$$\left.\begin{aligned} N_{i,1}(t) &= \begin{cases} 1 & (t_i \le t < t_{i+1}) \\ 0 & (t < t_i, t_{i+1} \le t) \end{cases} \\ N_{i,m}(t) &= \frac{t - t_i}{t_{i+m-1} - t_i} N_{i,m-1}(t) + \frac{t_{i+m} - t}{t_{i+m} - t_i + 1} N_{i+1,m-1}(t) \end{aligned}\right\}$$

$$P(t) \equiv (x(t), y(t), z(t)) = \frac{\sum_{i=0}^{n-1} N_{i,m}(t)\omega_i q_i}{\sum_{i=0}^{n-1} N_{i,m}(t)\omega_i} \qquad t_{m-1} \le t \le t_n$$

n :number of control points
m :order of NURBS curve
T :knot vector
t :parameter
N :B-spline basis function
q :coordinate of control points
P :coordinate of NURBS points
ω :weight parameter

As is shown in NURBS expression above, the NURBS curve is a mixture of the B-spline basis function and the coordinate of the control points. Moreover, few control points are needed to create a smooth curve. By using a CAD file format such as IGES (Initial Graphics Exchange Specification), an airfoil shape can be directly imported into the CAD software without any lack of information and modification is easy. The NURBS method can represent an airfoil with high camber and curvature, which is used in the civil jet plane and it leads to the rich design space. Then, we compared three ways of airfoil definition listed below to evaluate the accuracy of the NURBS airfoil representation method.

1) PARSEC
2) PARSEC + least square method
3) NURBS

For the three definitions above, parameter estimation for minimizing the geometry difference between the target airfoil and the estimated airfoil was conducted by the ARMOGA (Adaptive Range Multi Objective Genetic Algorithm)[6], which was a kind of the genetic algorithm as the optimizer. The objective function was as follows;

$$Obj = \sum_{i=1}^{n} \left| Zcal_i - Zorg_i \right|$$

In these problems, the ARMOGA generated 8 individuals at each generation and continued until the generation reached 400.

PARSEC

The 10 design variables (x_{up},z_{up},z_{xxup},x_{lo},z_{lo},z_{xxlo},α_{TE},β_{TE},r_{LElo}/r_{LEup},dy) used in this method is shown in Fig.1. The resultant airfoil shape is shown in Fig.2.

PARSEC + least square method

The airfoil was divided into two parts (thickness distribution + camber line). The former was expressed by the PARSEC-5 with 5

design variables (x_{up},z_{up},z_{xxup},β_{TE},dy), and the latter was expressed by the 5-th order polynomial function determined by the least squares method. The resultant shape is shown in Fig.3.

NURBS

The airfoil was expressed by the 5-th order NURBS curve. By careful investigation, the number of the control points and their distribution were determined. The 26 design variables (control points) used in this method is shown in Fig.4. The resultant airfoil is shown in Fig.5.

Evaluation

The R.M.S. of the geometry difference between the original airfoil and the estimated airfoils at three chord regions and total values are shown in Fig. 6 and Fig. 7, respectively. It is found that there are large errors at the leading edge with the PARSEC and the PARSEC + least square method. The PARSEC method used the leading edge radius to express the shape around the leading edge, therefore the flexibility of the shape at this region was limited and this caused errors at the region. On the other hand, the NURBS represented the shape of the original airfoil at whole region better than the PARSEC method.

The pressure distributions under transonic Mach number and constant Cl comparison of the original airfoil with ones estimated by each method are shown in Fig. 8. The airfoil generated by the PARSEC could not capture the suction peak at the leading edge, while one generated by the NURBS could express well. The R.M.S. of the geometry difference of each method seems not large, however, pressure distribution in transonic regime was so sensitive that small geometry deviation caused large discrepancy. Even the NURBS method needed more design variables than other methods, we adopted the NURBS method as the airfoil representation method in our study, because the pressure distribution around the leading edge including the suction peak determined high-speed performance of the civil jet plane.

2.2 Variable-Fidelity technique

In the engineering application, we can choose an optimizer depending on the optimization problem. In our previous work, we constructed an optimization tool using ARMOGA, which is one of the genetic algorithms (GA). The GA has the merit of finding a global optimum solution in the design space with discontinuity and multi-modalities. However, coupling GA with a high-fidelity aerodynamic evaluation tool such as Navier-Stokes method (CFD) requires much computational time and it is not practical in the aircraft development program.

Two solutions to overcome this problem are

1. Improving the way of selecting the population
2. Reduce time expected in the evaluation of the objective function.

For achieving the solution 1, we changed the way of selecting the population from one depending on the genetic information only to one, which related the objective function values and the design variables based on an approximation model.

The most widely used approximation model is a polynomial-based model [7], [8] because it is simple and easy to use. However, this model is not suitable for representing multi-modalities and non-linearity that often appear in the aerodynamic problem.

Recently, the Kriging model [9], [10], developed in the field of spatial and geostatistics, has gained popularity in this field. This model predicts the value of the unknown point using stochastic processes. Sample points are interpolated with the Gaussian random function to estimate the trend of the stochastic processes. It can reduce much time for objective function evaluation. However, such a prediction model includes some uncertainty in it. For the robust exploration of the global optimum solution, both the objective function value and its uncertainty should be considered at the same time. This concept is expressed in the criterion ‘expected improvement (EI)[11]’. The EI indicates the

probability of a point being optimum in the design space. By selecting the maximum EI point as an additional sample point, the improvement of the model and the robust exploration of the global optimum can be achieved at the same time. The Kriging model is constructed for each objective and constraint function. In the Kriging model for the objective function, the expected improvement is calculated, and in the Kriging model for the constraint, the probability of satisfying the constraint is calculated. Based on these values, an additional sample point for the balanced local and global search is selected using MOGA optimizer.

Though the computation time to construct the Kriging model is much shorter than that of the direct evaluations, it is likely to increase the optimization cycle to get a sufficient flexibility to represent the nonlinear and multimodal functions. For achieving the solution 2, the Variable-Fidelity [12] technique was introduced.

The Variable-Fidelity technique uses multiple fidelity models as the objective function evaluation method. The low-fidelity model such as a full potential method can evaluate an objective function at a short time, however the solution is not fully confident. On the other hand, though the high-fidelity model such as Navier-Stokes method takes much computation time, the solution is much confident than that of the low-fidelity model. Both models have different merits and demerits. The Variable-Fidelity technique does not depend on only a single fidelity model but also combine these models to make maximum use of the merits of both methods.

The key point of Variable-Fidelity technique is the construction of the "Bridge functions". The "Bridge functions" aim to correct the result from a low-fidelity model to one of a high-fidelity model.

Furthermore, the "Bridge functions" generate the result of uncalculated components. The example of the "Bridge functions" is shown below.

$$CL^{high-fidelity} = f(CL^{low-fidelity})$$

$$CL^{low-fidelity} = CL_{WING} + CL_{BODY}$$

$$CL_{BODY} = f(\alpha, CL_{WING})$$

In this example, CL_{WING} is the result of a low-fidelity model. Though CL_{BODY} is not calculated, it is estimated by using the angle of attack and CL_{WING}. In the early phase of the optimization, reliability of the "Bridge functions" is not sufficient and the correlation between the high-fidelity solution and the corrected low-fidelity solution is not necessarily high. In other words, if both solution matches, the "Bridge functions" are fully matured. In the optimization process, the "Bridge functions" are updated every time by using the objective function values of both low and high fidelity models.

The flowchart of the optimization process using a Kriging model with Variable-Fidelity technique is shown in Fig. 9.

1. Sample points to generate the original Kriging model are selected within the design space by using the Latin Hypercubes Sampling (LHS)[13]. Once LHS selects a point, the point is checked whether it satisfies the design constraints or not. If the point satisfies all constraints, the point is selected as a sample point and if not, the point is rejected.
2. All objective functions are evaluated by a low-fidelity model (full potential flow solver).
3. The Kriging models of each objective function are constructed. Then, by using MOGA, some points with higher EI value are picked up on the Kriging model.
4. All sample points, which are picked up in the previous step, are evaluated by both a low-fidelity model (full potential flow solver) and a high-fidelity model (Enler/NS solver).
5. The "Bridge Functions", connecting low and high fidelity solutions, are constructed
6. All objective function values of each sample point are recalculated with the "Bridge Functions" into high-fidelity values.
7. Go back to the 3rd step and this routine is iterated until the termination criterion is satisfied. In our current study, termination criterion was the maximum number of additional sample points.

As an example, Fig 10 shows our wing optimization result with structural constraints. The additional sample points are projected on a two-dimensional plane between the wing box weight and the cruise drag. As is shown in this figure, the rank of the drag and weight of each sample of the low-fidelity evaluations does not agree with that of the high-fidelity evaluations. On the other hand, the low-fidelity evaluations corrected by the "Bridge functions" are in good agreement with the high-fidelity evaluations. This result indicates that the “Bridge functions” are matured and the optimization using the corrected low-fidelity result is equivalent to one using the high-fidelity result.

The Variable-Fidelity technique using the “Bridge functions” can reduce the computational time of practical aircraft MDO problem drastically without loosing accuracy.

3 Engine-airframe integration

In the aircraft design, an engine-airframe integration problem is one of the most important design issues. Fig. 11(a) shows a shockwave generated around the inboard of the pylon and Fig. 11(b) shows the sectional pressure distribution at the pylon junction. This shockwave may lead to flow separation and cause buffet. In addition to this aerodynamic complexity, cruise drag, weight and flutter margin have to be taken into account. To overcome such complex design features, we extended the MDO tools to the engine-airframe integration.

In this kind of problem, it tends to take more time to modify the geometry than evaluation due to its geometrical complexity. Therefore, for a practical optimization, the automatic CFD and FEM mesh generator is the key points.

In our previous work based on a gradient method [14], [15], we developed the CFD mesh modification tool, which morphed the original geometry to the new geometry based on the spring analogy method. This tool was powerful and mandatory for gradient based optimization to obtain the geometry sensitivity, however, it was too complicated to avoid surface mesh distortion issue, and design space tended to be limited.

Therefore we switched the optimizer to MOGA which did not necessary require the geometry sensitivity information. Then we developed the automatic and robust mesh generator, which generated a mesh from scratch. This tool was very robust and assured a rich design space.

Fig.12 shows the process of the mesh generation of the wing-body-nacelle geometry. First, represent the wing, body and nacelle geometry, respectively. Next, combine the wing, nacelle and body into a single geometry. Finally, generate surface and the volume meshes. These operations are fully automated. The FEM mesh of the wing-body-nacelle geometry was also generated automatically as is shown in Fig.13. Because of its capability of generating the CFD and FEM mesh of the fully complex geometry, this tool enabled us to save much time for the geometry modification and the mesh generation. The time for CFD mesh generation was reduced to 1 minute from 1 day, and the time for FEM mesh generation was reduced to 10 seconds from 1 day.

To prove its validity and efficiency, the engine-airframe optimization problem was set as follows.

Design variables.

30 (26 variables for the airfoil shape of 2 sections and 4 for the wing twist)

Objective functions.

1. Minimize suction peak at the wing-pylon junction (which leads to minimize the buffet risk)
2. Minimize block fuel at a specific flight path (which leads to cruise drag reduction and wing box weight reduction)

Constraints.

1. Thickness of the wing geometry
2. Height of the front spar
3. Structural strength
4. Flutter speed

Fig. 14(a) shows the relationship between the suction peak at the wing-pylon junction and the cruise drag. Fig. 14(b) shows the relationship between the wing box weight and the cruise drag. Four typical geometries on the pareto front are extracted and the difference from the base geometry is shown in Table 1.

As is shown in Table 1, the candidate optimum geometry reduced the block fuel up to 3.4% from the baseline. Moreover the total optimization time is reduced to 10%.

4 Conclusion

To develop and improve high-fidelity aero-structural MDO tool to be used in the aircraft design, two techniques to improve the accuracy and efficiency were introduced.

1. The flexible wing representation method using the NURBS function was introduced. From the airfoil shape identification problem, it was proved that the NURBS airfoil representation method was much more accurate than the others such as PARSEC and polynomial function. It realized a rich design space for the optimization.
2. The Variable-Fidelity method coupling with the "Bridge Function" was introduced for the acceleration of the optimization. The three-dimensional wing-body optimization problem proved that our method was capable of reducing time up to 90% without any lack of accuracy.

As the next step, the wing-body MDO tool was extended to the engine-airframe integration. To overcome the geometrical complexity of the optimization, an automatic analysis model (CFD mesh and structural FEM mesh) generator was developed and applied. The optimization results proved that our MDO tool could be used as a practical design tool.

5 Acknowledgement

We would like to express special thanks to Mr. Kumano of Tohoku University, Mr. Takenaka and Mr. Morino of MHI for their sincere cooperation to the present work. We would also like to express special thanks to Dr. Ito of the University of Alabama at Birmingham for his cooperation to the automatic mesh generation tool development.

6 References

[1] NEDO website, "URL: http://www.nedo.go.jp/"

[2] Takenaka K, Obayashi S, Nakahashi K, and Matsushima K. The Application of MDO Technologies to the Design of a High Performance Small Jet Aircraft - Lessons learned and some practical concerns -. *AIAA-2005-0497*.

[3] Lepine J, Guibault F, Trepanier J-Y and Pepin. Optimized Nonuniform Rational B-spline Geometrical Representation for Aerodynamic Design of Wings *AIAA Journal*, Vol. 39, 2001.

[4] Hsiao-Yuan Wu, Shuchi Yang, Feng Liu and Her-Mann Tsai. Comparison of Three Geometric Representations of Airfoils for Aerodynamic Optimization *AIAA 2003–4095*.

[5] Oyama A, Obayashi S, Nakahashi K and Hirose N. Aerodynamic Wing Optimization via Evolutionary Algorithms Based on Structured Coding. *Computational Fluid Dynamics Journal*, Vol. 8, No. 4, 2000, pp. 570–577.

[6] Sasaki D, Obayashi S and Nakahashi K. Navier-Stokes Optimization of Supersonic Wings with Four Objectives Using Evolutionary Algorithm. *Journal of Aircraft*, Vol. 39, No. 4, 2002, pp. 621–629.

[7] Chen W, Allen J. K, Schrage D. P and Mistree F. Statistical Experimentation Methods for Achieving Affordable Concurrent Systems Design. *AIAA Journal*, Vol.35, No.5, pp.892-900, 1997.

[8] Simpson W T, Mauery M T, Korte J John and Mistree F. Comparison of Response Surface And Kriging Models for Multidisciplinary Design Optimization *AIAA paper 98-4755.*

[9] Jones R D, Schonlau M and Welch J. W. Efficient Global Optimization of Expensive Black-Box Function. *Journal of global optimization*, Vol.13, pp.455-492, 1998.

[10] Giunta A A, Watson L T. A Comparison of Approximation Modeling Techniques: Polynomial Versus Interpolating Models. *AIAA paper 98-4758*.

[11] Schonlau M. *Computer Experiments and Global Optimization.* Ph.D Dissertation, Statistic and Actuarial Science Dept., University of Waterloo, Waterloo, Ontario, 1997.

[12] Alexandrov N.M, Lewis R .M; Gumbert C R, Green L L, Newman P A. Optimization with Variable-Fidelity Models Applied to Wing Design. *AIAA-2000-0841*

[13] Mckay M. D., Beckman R. J. and Conover W. J. A Comparison of Three Methods for Selecting Values of Input Variables in the Analysis of Output from a Computer Code. *Technometric*, Vol. 21, No. 2, pp. 239-245, 1979.

[14] Salim K, Kim H.J and Nakahashi K. Aerodynamic Design of Wing-Body-Nacelle-Pylon Configuration. *AIAA2005-4856, 2005.*

[15] Ito Y, and Nakahashi K. Direct Surface Triangulation Using Stereolithography Data. *AIAA Journal*, Vol. 40, No. 3, pp. 490–496, 2002

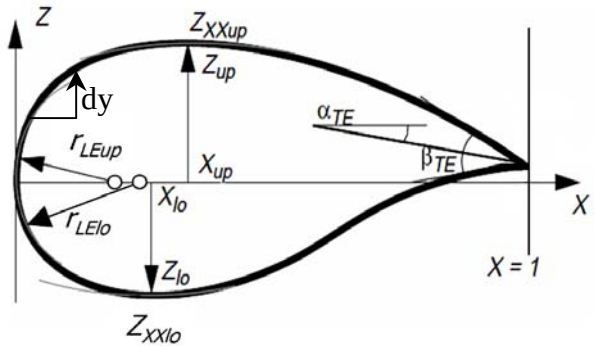

Figure 1. Illustration of the modified PARSEC airfoil shape defined by 10 design variables

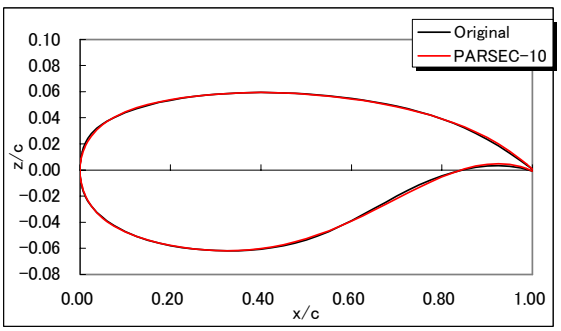

Figure 2. Airfoil representation result by PARSEC

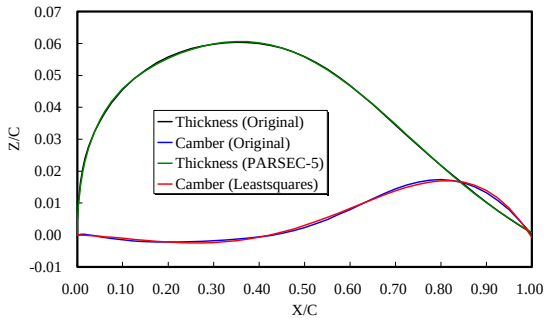

Figure 3. Airfoil representation result of PARSEC (thickness)+ Least squares (camber)

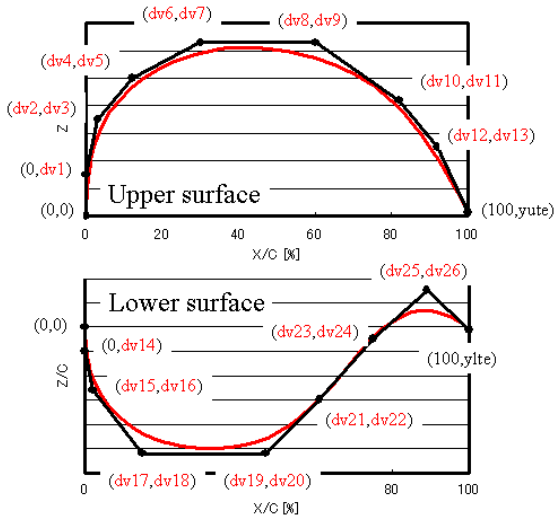

Figure 4. Design variables (control points) used in NURBS

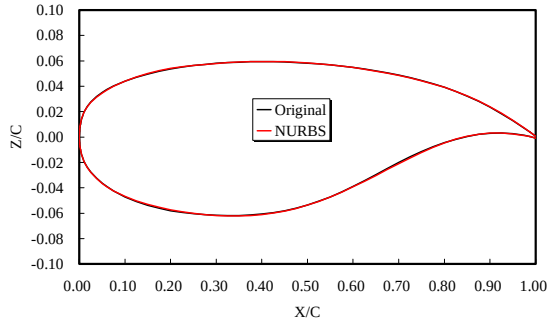

Figure 5. Airfoil representation result by NURBS

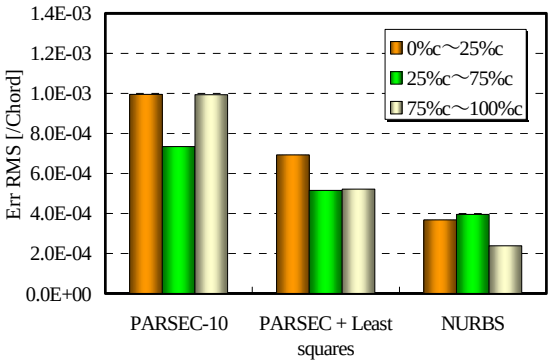

Figure 6. Comparison of R.M.S. of geometry difference at each chord region among each airfoil representation

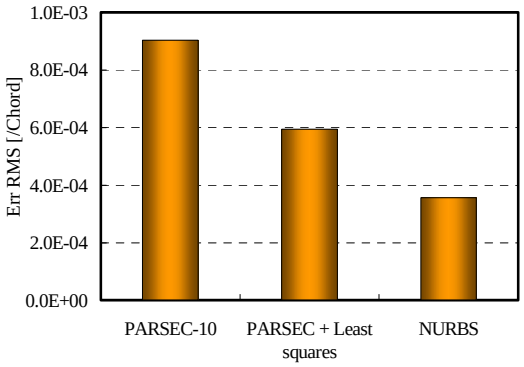

Figure 7. Comparison of R.M.S. of geometry difference among each airfoil representation

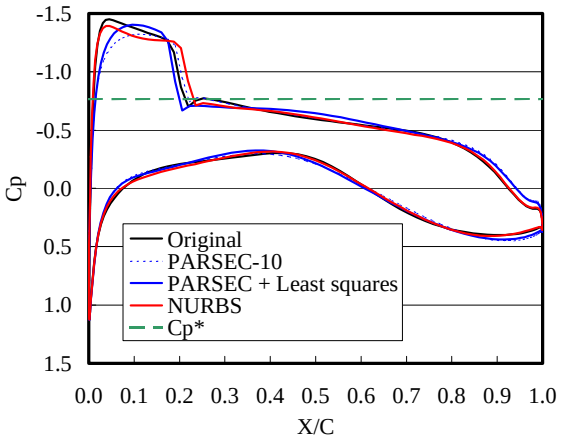

Figure 8. Comparison of airfoil surface pressure distributions by each representation (at transonic Mach number, constant CL)

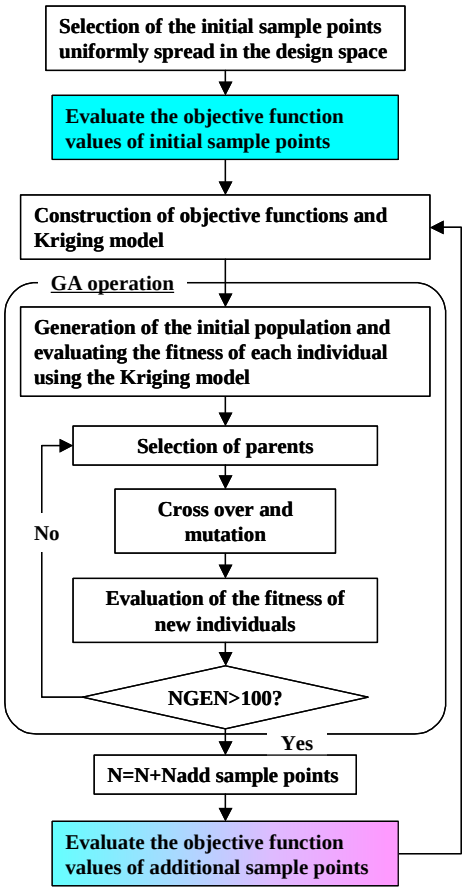

Construct the bridge functions and modify the objective function values computed with the low-fidelity method.

Figure 9 Optimization flow chart

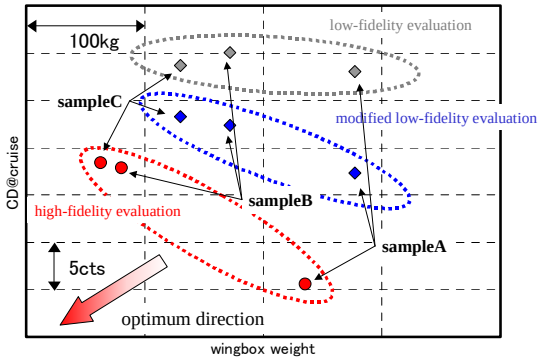

Figure 10. Additional sample points on two-dimensional plane between cruise drag and wing-box weight

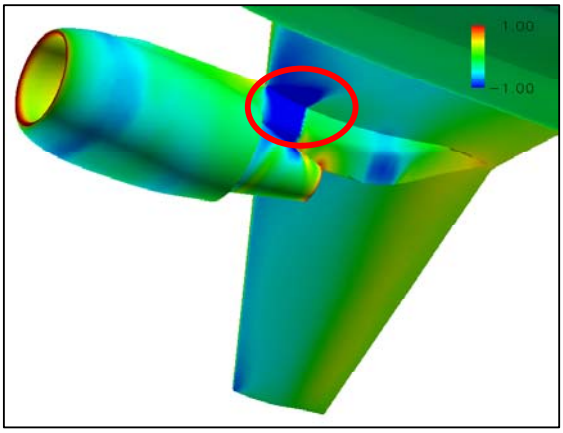

(a) surface pressure distribution

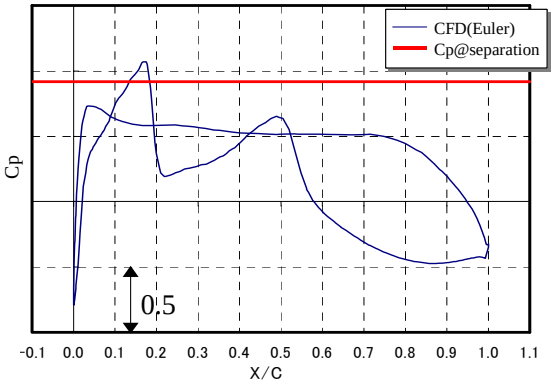

(b) sectional pressure distribution

Figure 11. pressure distribution at the junction of the pylon and the wing

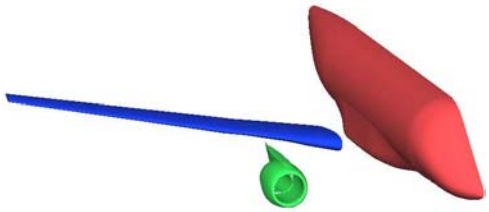

(a) represent each geometries

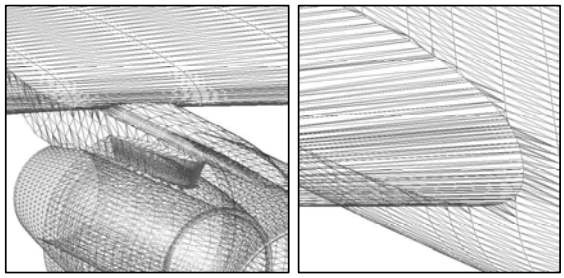

(b) combine all to one component

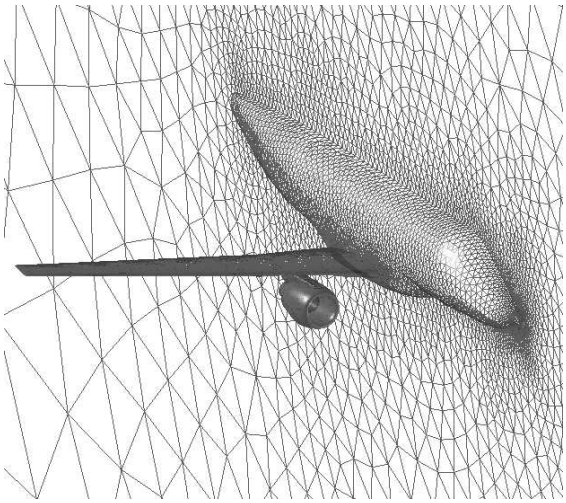

(c) generate surface grid and volumetric grid

Figure 12. the process of an automatic grid generation(CFD)

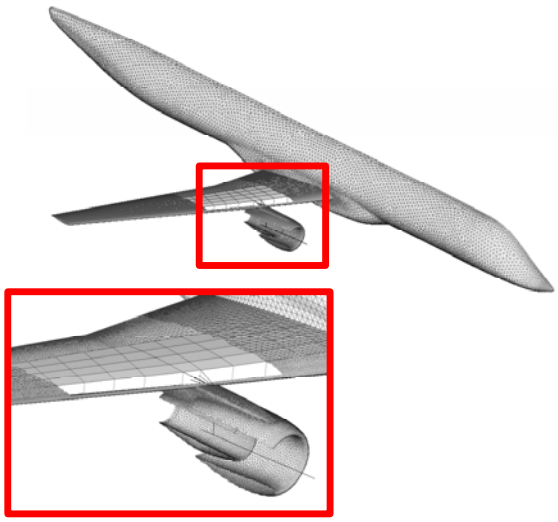

Figure 13. the FEM mesh

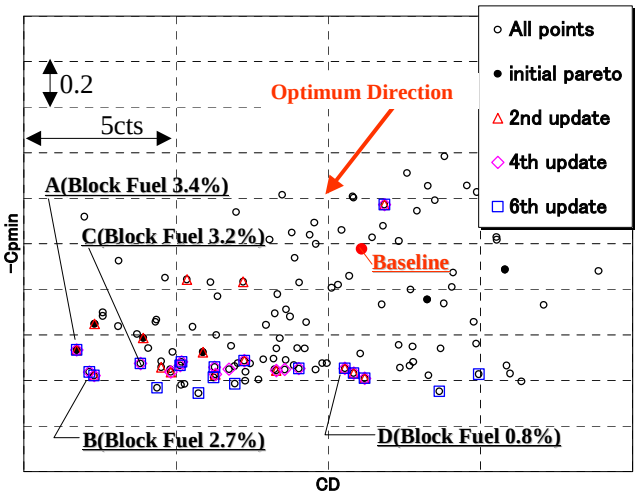

(a)CD vs -Cpmin

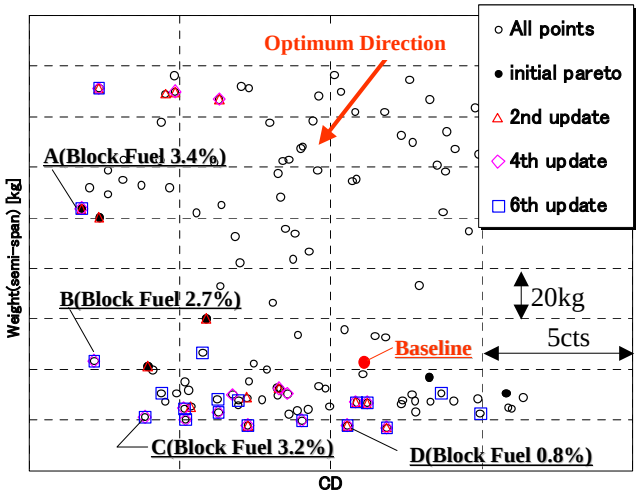

(b)CD vs Weight

Figure 14. the optimization result of the engine-airframe integration problem

Table 1. result of the extracted geometries

	Difference from Baseline		
	Drag(cts)	weight(kg)	Block Fuel(%)
A	−9	60.92	−3.4
B	−8	0.58	−2.7
C	−7	−21.58	−3.2
D	−1	−24.90	−0.8